Detection of deuterium trapping sites in tungsten by thermal desorption spectroscopy and positron annihilation spectroscopy

AUTHOR(S):

Sato, K.; Tamiya, R.; Xu, Q.; Tsuchida, H.; Yoshiie, T.

CITATION:

Sato, K. ...[et al]. Detection of deuterium trapping sites in tungsten by thermal desorption spectroscopy and positron annihilation spectroscopy. Nuclear Materials and Energy 2016, 9: 554-559

ISSUE DATE:

2016-12

URL:

http://hdl.handle.net/2433/218612

Nuclear Materials and Energy 9 (2016) 554–559

Contents lists available at ScienceDirect

Nuclear Materials and Energy

journal homepage: www.elsevier.com/locate/nme

Detection of deuterium trapping sites in tungsten by thermal desorption spectroscopy and positron annihilation spectroscopy

K. Sato[a,*], R. Tamiya[b], Q. Xu[b], H. Tsuchida[c], T. Yoshiie[b]

[a] Graduate School of Science and Engineering, Kagoshima University, Kagoshima-shi, Kagoshima, 890-0065 Japan
[b] Research Reactor Institute, Kyoto University, Kumatori-cho, Sennan-gun, Osaka, 590-0494 Japan
[c] Quantum Science and Engineering Center, Kyoto University, Uji-shi, Kyoto, 611-0011 Japan

ARTICLE INFO

Article history:
Received 16 November 2015
Revised 23 September 2016
Accepted 24 September 2016
Available online 14 October 2016

Keywords:
Tungsten
Hydrogen isotopes
Thermal desorption spectroscopy
Positron annihilation
Defects
Ion implantation

ABSTRACT

Thermal desorption spectroscopy (TDS) of tungsten implanted with D_2^+ ions was performed after irradiation with 8 MeV-electrons, 5.0 keV-D_2^+, and 6.0 MeV-Fe^{3+}. The release peak temperatures of the TDS spectra are discussed. Positron annihilation lifetime (PAL) measurements of electron-irradiated tungsten were also performed, showing that single vacancies migrate a sufficient distance to arrive at a sink or meet interstitial-type defects during annealing at 673 K. A decrease in the PAL was detected for single vacancies that contain deuterium atoms. The peak temperature of deuterium release from dislocations was lower than that from single vacancies. In samples irradiated with 6.0 MeV-Fe^{3+}, the effect of Fe contamination on deuterium trapping and the deuterium release from voids were detected. These tendencies correspond to previous works.

1. Introduction

In a fusion reactor, plasma-facing materials (PFMs) must withstand the damage produced by plasma particles at energies ranging from several electron volt to several kiloelectron volt [1], heat loads from the plasma, and neutrons with high energy, high flux, and high fluence. Therefore, important criteria for the selection of PFMs are high melting point, high thermal conductivity, and low sputtering erosion. High-Z materials such as tungsten, and molybdenum, together with low-Z materials such as carbon, carbon fibre composites and beryllium have been selected as PFMs due to outstanding thermal properties and erosion resistance. The plasma-induced erosion in high-Z materials, especially tungsten, is considerably lower than that in low-Z materials. However, high-Z materials have a far lower tolerance to impurity concentrations within the plasma [2], as the radiative power loss of the plasma is proportional to the square of the charge number of impurity ions. Another disadvantage is bubble formation, where hydrogen isotopes are retained in vacancy-type defects in PFMs [3,4], which is a critical problem for fusion reactors. Thus, it is very important to determine the interactions between vacancy-type defects and hydrogen isotopes.

Positron annihilation spectroscopy (PAS) is a very powerful tool for detecting vacancy type defects. Many research groups adopted PAS to investigate the irradiation effects in tungsten [5–10]; however, they mainly performed PAS after irradiation. Van Veen et al. and de Vries et al. reported the change in the positron annihilation lifetime (PAL) of hydrogen decorated vacancies and voids by annealing in tungsten [11,12]. In this study, the size of vacancy-type defects in tungsten was evaluated from PAL measurements, which were performed before and after deuterium charging to identify the type of pre-existing defects (deuterium trapping sites) and obtain the change in the PAL of vacancies by deuterium trapping. Thermal desorption spectra of deuterium were also obtained after deuterium charging. The trapping sites and peak temperatures of deuterium release from tungsten were identified from these results.

2. Experimental procedure

High purity tungsten (99.95%, A.L.M.T. Corp.) samples were employed in this study. Samples with diameters of 5 mm were punched from 0.2 mm thick tungsten sheets and annealed at 1773 K for 1 h in a vacuum ($<10^{-4}$ Pa) to facilitate recrystallization. All samples were electropolished before and after annealing to remove any oxidation. As mentioned in the next paragraph, electron irradiation was performed with water cooling. An oxidation layer was formed on the surface during electron irradiation and was re-

* Corresponding author. Fax +81-99-285-8265.
E-mail address: ksato@mech.kagoshima-u.ac.jp (K. Sato).

http://dx.doi.org/10.1016/j.nme.2016.09.014

Table 1
Sample list and experimental conditions.

Sample	Annealing condition	Irradiation condition	D_2^+ ion implantation
As-received	–	–	1 keV 1.0×10^{22} /m^2
Well-annealed	1773 K for 1 h	–	1.0– 1.5 keV 5.0×10^{21} /m^2
Dislocation	1273 K for 5 h	–	1 keV 1.0×10^{22} /m^2
Electron-irr.	1773 K for 1 h	8 MeV electrons 9.4×10^{21} /m^2 (333 K) 5 keV D_2^+ ions	1 keV 1.0×10^{22} /m^2
D_2^+-irr. (R.T.)	1773 K for 1 h	1.0×10^{22} /m^2 (room temperature.)	–
D_2^+-irr. (H.T.)	1773 K for 1 h	5 keV D_2^+ ions 1.0×10^{22} /m^2 (673 K)	1 keV 1.0×10^{22} /m^2
Fe^{3+}-irr.	1773 K for 1 h	6 MeV Fe^{3+} ions 2.3×10^{23} /m^2 (573 K)	1 keV 1.0×10^{22} /m^2

moved by electropolishing. All samples were electropolished after annealing so thermal desorption spectroscopy (TDS) could be performed under the same surface conditions. Defects were introduced by irradiation with electrons, D_2^+ ions and Fe^{3+} ions.

The electron irradiation was performed at 8 MeV at doses to 2.1×10^{21} and 9.4×10^{21} /m^2 (7.1×10^{-6} and 3.2×10^{-5} dpa) at 333 K using the Electron Linear Accelerator of the Research Reactor Institute, Kyoto University. Water cooling was adopted to remove beam heating, and the sample temperature was measured with a thermocouple. For dose calculations, we applied linear interpolation to the values listed in reference [13] to obtain the atomic displacement cross section of 70.4 barns. Ogorodnikova et al. reported the cross section of 34 barns in the case of 3.5 MeV electron irradiation [14]. Their value is almost equal to the atomic displacement cross section with the displacement threshold energy of 84 eV for 3.5 MeV electron irradiation [13]. Therefore, the displacement threshold energy of 84 eV was used for the dose calculation of electron irradiation. Deuterium ion irradiation was performed with 5 keV D_2^+ ions at up to 1.0×10^{22} /m^2, providing 2.8 dpa at the defect peak, 5 nm from the surface, at room temperature and 673 K using the low-energy ion irradiation system of the Research Reactor Institute, Kyoto University. Heavy ion irradiation was performed with 6 MeV Fe^{3+} ions at up to 2.3×10^{19} /m^2, providing 1.9 dpa at the defect peak, 11 μm from the surface, at 573 K at Quantum Science and Engineering Center, Kyoto University. The irradiation doses and defect peaks of the ion irradiation were obtained by analysing the results of an SRIM simulation [15] with the Quick Kinchin-Pease option [16].

Samples containing only dislocations were prepared by annealing the as-received samples at 1273 K for 5 h. Table 1 lists the details for each sample and the experimental conditions employed. The untreated sample and the samples annealed at 1723 K for 1 h and at 1273 K for 5 h are referred to as the “as-received”, “well-annealed”, and “dislocation” tungsten samples, respectively. The irradiated samples are referred to as the “Electron-irr.”, “D_2^+-irr. (R.T.)”, “D_2^+-irr. (H.T.)” and “Fe^{3+}-irr.” in accordance with the irradiation conditions shown in Table 1.

D_2^+ ions were implanted (1 keV, 1×10^{22} /m^2) at room temperature to the as-received, dislocation, well-annealed, electron-irr., D_2^+-irr. (H.T.), and Fe^{3+}-irr. samples. Since we could not obtain any peaks in the TDS spectrum of the D_2^+-irr. (H.T.) sample after 5 keV D_2^+ irradiation, subsequent 1 keV D_2^+ irradiation was needed. On the other hand, because the D_2^+-irr. (R.T.) sample sufficiently retained D atoms after irradiation, we did not conduct 1 keV D_2^+ irradiation. Thermal desorption spectroscopy (TDS) was conducted from room temperature to 1523 K at a heating rate of 1 K/s to study the behaviour of deuterium release from tungsten defects. The samples were transferred from the D_2^+ ion implantation apparatus to the TDS instrument in a vacuum chamber. However, the samples were exposed to air for approximately 10 min while fixed to the sample holder of the TDS instrument. The PAL measurements were performed at room temperature using a fast-fast coincidence system with a time resolution of 190 ps (full width at half maximum; FWHM) [17]. We used Na-22 as the positron source. The energy spectrum of positrons emitted from Na-22 is broad up to an energy of approximately 540 keV [18]. The maximum penetration depth in tungsten was about 100 μm using the so-called Makhov distribution [19]. The PAL spectra were collected with a total count of $1.0 - 1.5 \times 10^6$ and were analysed using the PALSfit program [20]. The positron annihilation lifetime spectra of well-annealed and electron-irr. W are shown in Fig. 1. The errors given in Table 2 denote the standard deviations obtained in the decomposition of the PAL spectra, which are not dependent on the time resolution of the experimental system. The total amount of residual defects can be derived from the mean positron lifetime (τ_m). The amount of positron annihilation that occurs in the matrix can be determined from the short lifetime component (τ_1), the size of vacancy-type defects can be derived from the long lifetime component (τ_2), and the density can be obtained from the relative intensity of the long lifetime component (I_2). When vacancy clusters grow, the positron lifetime increases. Table 2 gives the positron annihilation lifetimes for the as-received, dislocation, well-annealed, and electron-irr. tungsten. The long lifetime component, τ_2, of 149 ps for the dislocation sample was shorter than that calculated for single vacancies, 161 – 200 ps [21, 22], indicating that the sample contains no vacancy clusters or single vacancies. The short lifetimes of 19 ps (dislocation) and 85 ps (electron-irr.) denote the lifetime of positron disappearance not only at the matrix but also from it (migration to the defect site). In the two-state trapping model [23–25], the short lifetime τ_1 is expressed as $\tau_1 = 1 / (\lambda_f + \kappa)$ (κ: the trapping rate to defects). As $\tau_f = 1 / \lambda_f$

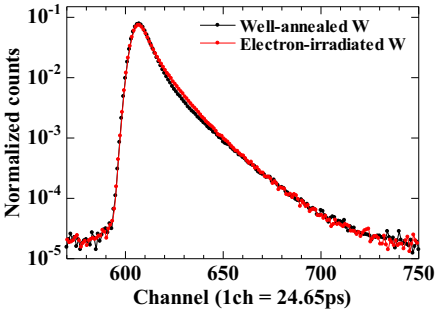

Fig. 1. Positron annihilation lifetime spectra of well-annealed and electron-irr. tungsten. The dose of electron irradiation was 3.2×10^{-5} dpa, and the spectrum after electron irradiation changed at around 630 ch.

Table 2
Positron annihilation lifetime for as-received, dislocation, well-annealed and electron-irr. tungsten. τ_m, τ_1, τ_2, and I_2 denote mean, short, and long lifetimes, and long lifetime intensity, respectively.

Sample	τ_m (ps)	τ_1 (ps)	τ_2 (ps)	I_2 (%)
As-received	175 ± 1	163 ± 1	400 ± 1	6 ± 1
Dislocation	148 ± 1	19 ± 8	149 ± 1	94 ± 1
Well-annealed	109 ± 1	–	–	–
Electron-irr.	127 ± 1	85 ± 2	173 ± 4	42 ± 3

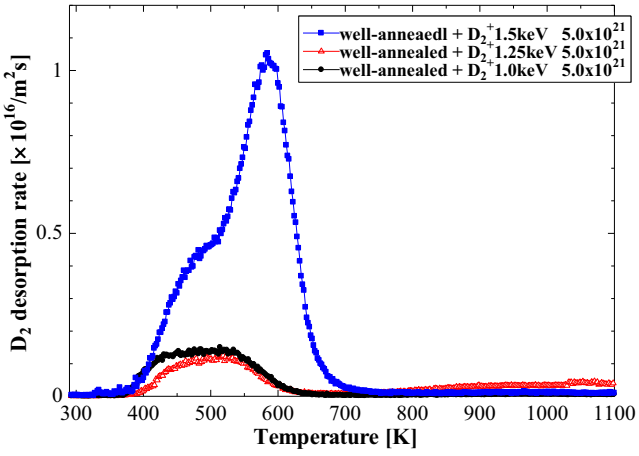

Fig. 2. TDS spectra for well-annealed tungsten with various energies of D_2^+ ion-implantation (1.0 – 1.5 keV). Implantation fluence was 5.0×10^{21} /m^2.

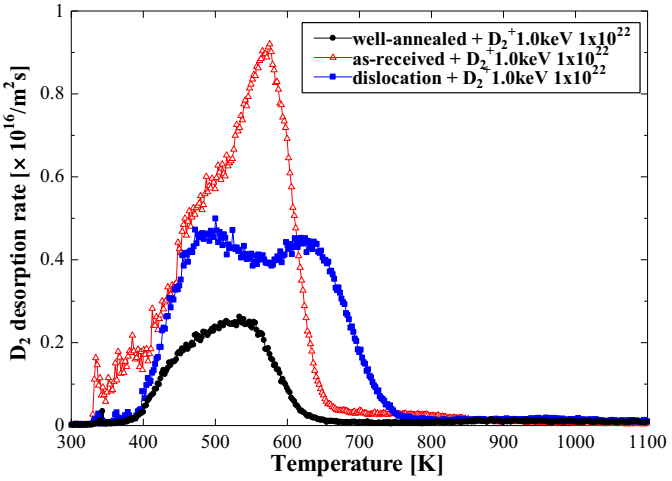

Fig. 3. TDS spectra for as-received, well-annealed, and dislocation tungsten. The 1.0 keV D_2^+ ions were implanted with a fluence of 1.0×10^{22} /m^2 after heat treatments.

denotes the lifetime of well-annealed tungsten (about 110 ps), τ_1 can be less than the lifetime of the matrix. The PAL measurements were not applied to D_2^+-irr. and Fe^{3+}-irr. tungsten. Because the defect distribution resulting from ion irradiation is shallower than the positron penetration depth, it is difficult to obtain valuable information about the irradiation-induced defects. TEM observations were carried out using a 200 keV electron microscope (JEM2010) for D_2^+-irr. (R.T.) and D_2^+-irr. (H.T.).

3. Results and discussion

3.1. As-received and well-annealed tungsten

Fig. 2 shows TDS spectra for well-annealed tungsten implanted with D_2^+ ions at various implantation energies in the range of 1.0 to 1.5 keV (fluence: 5.0×10^{12} /m^2). Ogorodnikova et al. suggest that deuterium ion implantation with low energy creates dislocations, vacancies and vacancy clusters near the surface [26,27]. In this study, however, no peak was obtained at 600 K for energies less than 1.5 keV, which suggests that, for implantation energies of 1.0 and 1.25 keV, deuterium atoms are trapped in intrinsic defects (e.g. dislocations). For an implantation energy of 1.5 keV, deuterium atoms are trapped in defects formed by the implantation itself (e.g. vacancies) [27,28].

Fig. 3 shows the TDS spectra of the as-received, well-annealed, and dislocation tungsten. From the PAL measurement of the as-received sample, the short lifetime component, τ_1, of 163 ps denotes the mixed PAL of dislocations and single vacancies, which could not be decomposed into two components even if the machines with the best time resolution were used. The long lifetime component, τ_2, of 400 ps denotes the PAL of vacancy clusters. Therefore, the as-received sample contained dislocations, single vacancies, and vacancy clusters, and the dislocation sample contained mainly dislocations. Apart from the defects formed by implanted low-energy ions, other defects (dislocations and/or vacancy clusters) existed prior to D_2^+ ion implantation. Deuterium atoms were trapped in these pre-existing defects, which then had an effect on TDS spectra. In the as-received sample, one peak is observed at 580 K with a shoulder around 500 K. In dislocation tungsten, two peaks are observed at 480 and 630 K. It is expected that peaks around 460 ± 20 K, 555 ± 15 K, and 640 ± 10 K were caused by the dislocations, single vacancies, and vacancy clusters, respectively. In the dislocation sample, residual open-volume defects that interacted with the strain field of dislocations (e.g. vacancies trapped at edge dislocations [29]) trap many deuterium atoms, and vacancy clusters may be formed by the mechanism proposed by Ogorodnikova et al. in low-energy ion implantation [26]. Therefore, the low- and high-temperature peaks are due to the dislocations and vacancy clusters, respectively.

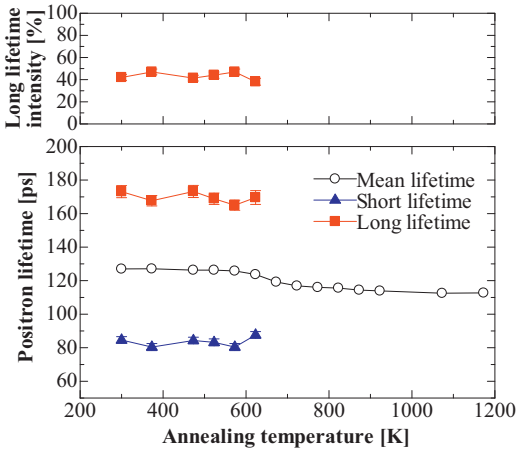

Fig. 4. Isochronal annealing behaviour of electron-irr. tungsten for an annealing time of 1 h. The irradiation dose of electrons was 3.2×10^{-5} dpa.

3.2. Tungsten irradiated with electrons at 8 MeV

Fig. 4 shows the isochronal annealing behaviour of electron-irradiated tungsten for an annealing time of 1 h. The maximum PKA energy from electron irradiation is expressed as $E_{p,max} = 2E(E + 2m_0c^2)/M_2c^2$, where m_0 is the electron rest mass and c is the speed of light. The maximum PKA energy from 8 MeV-electrons is 836 eV, which is sufficiently high to cause a collision cascade. From reference [13], the ratio of the cross section for the occurrence of a collision cascade, 97 barns, to that for purely Frenkel pair formation, 70 barns, is approximately 1.4. Thus, more than two-thirds of the electrons introduce Frenkel pairs, and even if the collision cascade occurs, the cascade size is small due to the small PKA energy. After irradiation, a long positron lifetime of 173 ps is obtained, indicating single vacancies, and that vacancy clusters are not formed, even by the collision cascade. After annealing at 673 K, the mean lifetime begins to decrease and the PAL spectrum cannot be decomposed into two components, indicating that single vacancies begin to migrate a sufficient distance to arrive at a sink or meet interstitial-type defects during the annealing. The vacancy

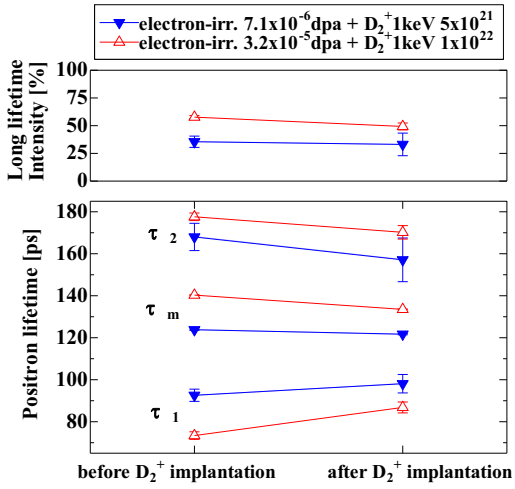

Fig. 5. Variation in positron annihilation lifetime for electron-irr. tungsten before and after D_2^+ ion implantation. The irradiation dose of electrons was 7.1×10^{-6} and 3.2×10^{-5} dpa. The 1.0 keV D_2^+ ions were implanted with fluences of 5.0×10^{21} and 1.0×10^{22} /m^2 after electron irradiation. The terms τ_m, τ_1, and τ_2 denote the mean, short, and long lifetimes, respectively.

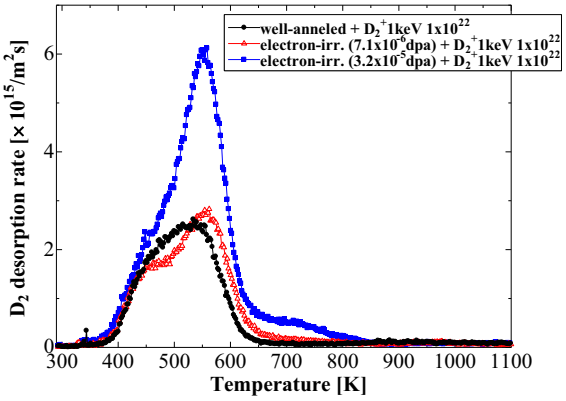

Fig. 6. TDS spectra for electron-irr. tungsten. The irradiation doses of electrons were 7.1×10^{-6} and 3.2×10^{-5} dpa. After electron irradiation, 1.0 keV D_2^+ ions were implanted with a fluence of 1.0×10^{22} /m^2.

migration energy in tungsten is 1.70 eV [30]. The average vacancy jump distance at 673 K for 1 h is 82 atomic distances or 11.4 nm. Since there are more than 10^6 atoms present within a radius of 82 atomic distances, if the interstitial-type defect concentration is more than 10^{-6}, vacancies can meet interstitial-type defects during annealing. Since the tungsten used in this study is not extremely high purity, irradiation-induced interstitials could be trapped at impurities, and interstitial clusters formed during irradiation. They were also affected by impurities, and their motion was restricted. Sato et al. reported that in nickel binary alloys during neutron irradiation the interstitial clusters are trapped at impurities, promoting vacancy annihilation, and suppressing the growth of vacancy clusters [31]. In electron-irr. tungsten, if vacancies were not annihilated, they would agglomerate and the long positron lifetime also would increase. Therefore, similar to nickel alloys, vacancies in tungsten meet the interstitial clusters trapped at impurities and are annihilated. In this study, the irradiation dose was not high. After annealing at 673 K, even if vacancy clusters were formed, their concentration would be lower than the detection limit of the PAS ($\sim 10^{-6}$). In this case, the lifetime spectra cannot be decomposed into two components. If the irradiation dose is higher, the formation of vacancy clusters should be detected as reported by Debelle et al. [9].

Fig. 5 shows the variation in the PAL for electron-irradiated tungsten before and after D_2^+ ion implantation. The vacancies trap deuterium atoms, and the long positron lifetime decreases, as per the tendencies observed in previous experiments and simulations [11,12,22]. The long positron lifetime did not change so significantly in the present study. Since positrons penetrate to depths of approximately 100 μm, the average defect size and density in the penetration depth can be obtained by PAS. If samples do not contain any defects, implanted deuterium atoms are expected to diffuse up to a depth of 79 μm at room temperature during 10 h of irradiation, using migration energy of 0.39 eV [32]. However, deuterium atoms cannot diffuse to 79 μm because vacancies trap deuterium atoms [33,34]. Vacancies containing deuterium atoms do not exist in the whole range of 100 μm positron penetration depth. Therefore, a part of positrons is annihilated at vacancies containing deuterium atoms, and the other part of positrons is annihilated at vacancies not containing deuterium atoms. Therefore, if hydrogen isotopes can be introduced to all areas of the samples and vacancies capture more hydrogen isotopes, the PALs will be significantly decreased, as obtained in simulation [22]. This phenomenon will be studied in the near future. The increase of the short lifetime in Fig. 5 is explained by the change in the positron trapping rate to defects (κ).

Fig. 6 shows the TDS spectra of tungsten irradiated with electrons at doses of 7.1×10^{-6} and 3.2×10^{-5} dpa. Deuterium retention of electron irradiation at a dose of 7.1×10^{-6} dpa is almost the same as that of the well-annealed sample. We do not clearly know whether the deuterium atoms were trapped at electron-induced or ion-induced vacancies at 7.1×10^{-6} dpa. The spectrum for dose 3.2×10^{-5} dpa displays a peak around 550 K, a shoulder around 450 K, and a long tail in the 750 K region. The peak around 550 K and the shoulder around 450 K increase with increasing irradiation dose. Deuterium atoms were also trapped at small interstitial clusters (dislocation loops) and single vacancies formed by electron irradiation. Dislocation loops were not detected by the PAL measurements; however, the peak caused by them was obtained by TDS. Deuterium atoms are intensively trapped by dislocations. In contrast, positrons are not sensitive to detect dislocations. It is expected that the tail around 750 K is caused by the low-energy ion-induced vacancy clusters. The density of irradiation-induced dislocation loops increases with increasing the irradiation dose. We expect that the low-energy ion-induced vacancy clusters are formed by the strain field of dislocation loops as mentioned in Section 3.1.

3.3. Tungsten irradiated with D_2^+ at 5 keV and Fe^{3+} at 6 MeV

Fig. 7 shows the TDS spectra of tungsten irradiated with 5 keV D_2^+ ions at room temperature (D_2^+-irr. (R.T.)) and 673 K (D_2^+-irr. (H.T.)). The irradiation temperature was changed to introduce vacancy clusters of different sizes. The D_2^+-irr. (R.T.) sample displays one peak at 550 K and two shoulders around 450 and 650 K, while the D_2^+-irr. (H.T.). sample displays two peaks at 440 and 620 K. Fig. 8 shows TEM images of tungsten irradiated with 5 keV D_2^+ ions at (a) room temperature and (c) 673 K. Figs 8(b) and (d) show enlarged photographs of the squares in (a) and (c), respectively. No dislocations are shown in Fig. 8, and all of the dark circles indicated by the arrows are dislocation loops. The dislocation loop density is clearly higher in the room temperature irradiation case. The peak of the room temperature irradiation around 450 K is higher than that of the 673 K irradiation. The peaks around 550 K and 650 K denote the release of deuterium from single vacancies and vacancy clusters, respectively. In the 673 K irradiation, the peak at 620 K is composed of two Gaussian functions (see Section 3.4). This result indicates that both single vacancies and vacancy clusters are formed. Because of the high irradiation temper-

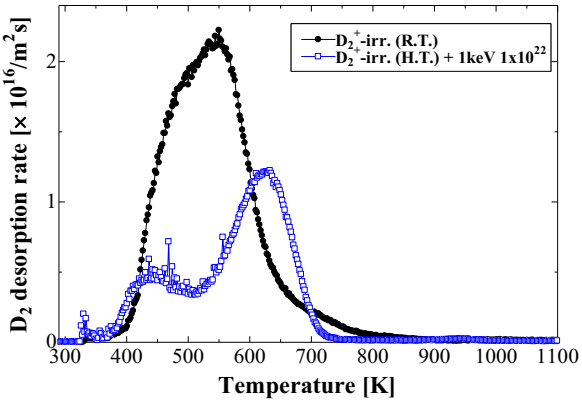

Fig. 7. TDS spectra for D_2^+-irr. (R.T.) and D_2^+-irr. (H.T.) tungsten. Since, after 673 K irradiation, peaks of D_2 were not detected by TDS, 1.0 keV D_2^+ ions were implanted with a fluence of 1.0×10^{22} /m^2.

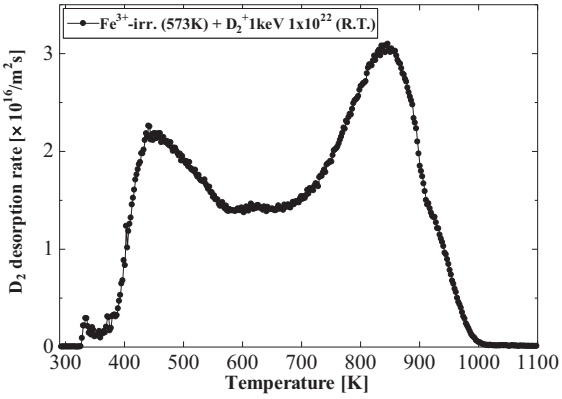

Fig. 9. TDS spectrum for Fe^{3+}-irr. tungsten (Fe^{3+}-ion-irradiation temperature: 573 K). After Fe^{3+} ion irradiation, 1.0 keV D_2^+ ions were implanted with a fluence of 1.0×10^{22} /m^2.

ature, the concentration of vacancy clusters is higher in the 673 K irradiation than in the room temperature irradiation. Therefore, the peak around 640 K caused by vacancy clusters is also higher in the 673 K irradiation than in the room temperature irradiation. Vacancy mobility is not so high that single vacancies can remain under the irradiation temperature of 673 K. In these cases, even if the low-energy ion-induced vacancy clusters are formed, the density of them should be so lower than that of irradiation-induced vacancy clusters.

After Fe^{3+} ion irradiation, the mean positron lifetime increased by a few picoseconds. However, the lifetime spectrum cannot be decomposed into two components. The TDS spectra of tungsten irradiated with 6 MeV Fe^{3+} ions at 573 K (Fe^{3+}-irr.), as shown in Fig. 9, displays two peaks at 440 and 830 K and a broad tail between 550 and 750 K. Because 6 MeV Fe^{3+} ions create larger cascade damage than 5 keV D_2^+ ions do and because a high temperature (573 K) promotes faster vacancy migration than at room temperature, we expect the formation of large voids. Causy et al. [35] and Ogorodnikova et al. [36] reported that the dissociation energy of hydrogen chemisorbed on the walls of the voids is 1.8 – 2.1 eV. It is expected that voids formed by the 6 MeV Fe^{3+} irradiation caused the peak around 830 K, and dislocation loops, single vacancies, and vacancy clusters caused the other peaks and tails. However, Barton et al. reported that, in Cu^+ ion-irradiated tungsten, Cu contaminations produce a broad TDS spectrum [37]. In this study, Fe contaminations can/may affect the TDS spectrum.

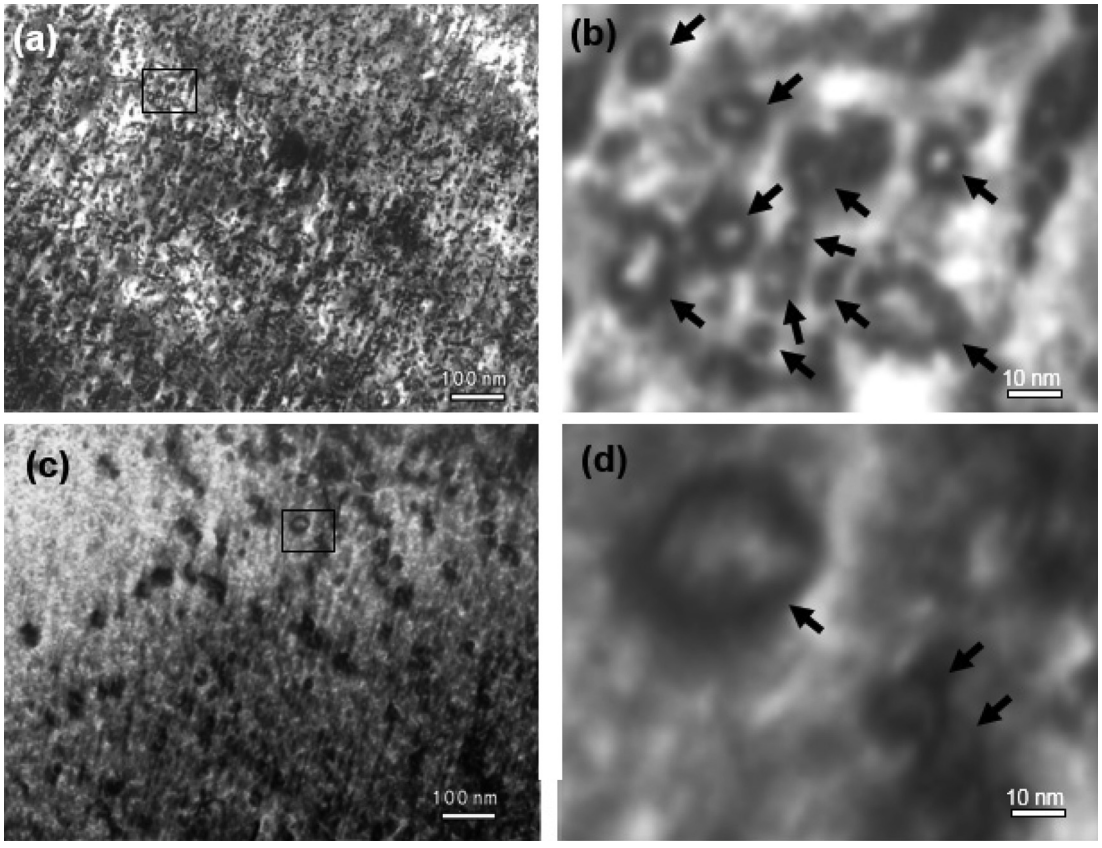

Fig. 8. TEM images of tungsten irradiated with 5 keV D_2^+ ions at (a) room temperature and (c) 673 K. (b) and (d) show enlarged photographs of the squares in (a) and (c), respectively. Arrows denote dislocation loops.

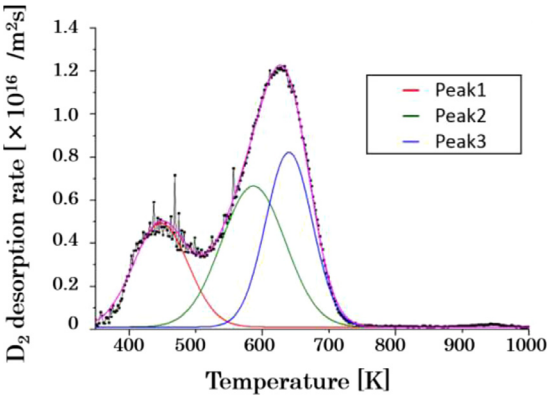

Fig. 10. Peak separation of the TDS spectrum for D_2^+-irr. (H.T.) tungsten. A series of Gaussian functions was used.

Table 3
Peak temperatures after peak separation (Heating rate: 1 K/s). Except for D_2^+-irr. (R.T.), 1 keV D_2^+ ion implantation with the fluence of 1×10^{22} /m^2 was performed after introducing the defects or heat treatments. Peak temperatures of the TDS spectra changed depending on the ion energy, heating rate, fluence, etc.

Sample	Peak temperature (K)			
	Peak I	Peak II	Peak III	Peak IV
As-received	470	570	–	–
Dislocation	490	–	630	–
Electron-irr.	460	560	–	–
D_2^+-irr. (R.T.)	460	550	650	–
D_2^+-irr. (H.T.)	450	580	640	–
Fe^{3+}-irr.	450	–	630	850

3.4. Identification of deuterium trapping sites

The TDS spectra peaks were separated and fitted with a series of Gaussian functions. Fig. 10 shows an example of peak separation of the TDS spectrum for tungsten irradiated with 5 keV D_2^+ ions at 673 K. Table 3 shows the peak temperatures obtained from the peak separation. Four regions are obtained: the first peak (peak I) at 450 – 490 K, the second (peak II) at 550 – 580 K, the third (peak III) at 630 – 650 K, and the fourth (peak IV) at 850 K. We expect that peaks I–IV are caused by dislocations (dislocation loops), single vacancies, vacancy clusters, and chemisorption of deuterium atoms on the surface of large voids, respectively. In previous works [26–28,36], peaks caused by single vacancies and vacancy clusters are not decomposed, and the trap energies of deuterium in vacancy clusters and atomic deuterium with single vacancies are almost the same (~1.4 eV). In this study, peak II and III are separated, which may be caused by the difference of the heating rate, the ion energy, fluence and so on, or by the essential difference of the trap energies of vacancies and vacancy clusters such as α-Fe [38]. In future research, we will analyse the vacancy cluster size formed by the ion irradiation by using the slow positron beam technique, and we will study the relationship between vacancy cluster size and TDS spectra in more detail than in previous work [10].

4. Concluding remarks

TDS and PAL measurements of tungsten irradiated with 8 MeV electrons, 5.0 keV D_2^+ ions and 6 MeV Fe^{3+} ions were conducted. From the results of this work, we arrived at the following conclusions.

1. The PAL measurements indicated that single vacancies start to migrate a sufficient distance to meet interstitial-type defects at 673 K.
2. The change in PAL of single vacancies by the trap of deuterium atoms was detected from PAL measurements.
3. The TDS experiments revealed peaks in four different intervals depending on the material preparation and irradiation conditions, which are caused by dislocations, single vacancies, vacancy clusters and the chemisorption of deuterium on the surface of voids, respectively. These results support previous works [26–28,36]. However, more precise analysis of peak II and III is necessary.

References

[1] V. Kotov, A. Litnovsky, A.S. Kukushkin, D. Reiter, A. Kirschner, J. Nucl. Mater. 528 (2009) 390–391.
[2] G. McCracken, P. Stott, Nucl. Fusion 19 (1979) 889.
[3] H. Iwakiri, K. Morishita, N. Yoshida, J. Nucl. Mater. 135 (2002) 307–311.
[4] F. Sefta, K.E. Hammond, N. Juslin, B.D. Wirth, Nucl. Fusion 53 (2013) 073015.
[5] V.S. Subrahmanyam, P.M.G. Nambissan, P. Sen, Solid State Comm 89 (1994) 523.
[6] H. Eleveld, A. van Veen, J. Nucl. Mater. 1421 (1994) 212–215.
[7] S.G. Zhu, Y.J. Xu, Z.Q. Wang, Y.N. Zheng, D.M. Zhou, E.P. Du, D.Q. Yuan, M. Fukuda, M. Mihara, K. Matsuta, T. Minamisono, J. Nucl. Mater. 343 (2005) 330.
[8] W.M. Shu, A. Kawasuso, Y. Miwa, E. Wakai, G.N. Luo, T. Yamanishi, Phys. Scr. T128 (2007) 96.
[9] A. Defelle, M.F. Barthe, T. Sauvage, J. Nucl. Mater. 376 (2008) 216.
[10] F. Liu, Y.P. Xu, H.S. Zhou, X.C. Li, Y. Song, C.H. Zhang, Q.C. Li, C.Q. He, G.N. Luo, Nucl. Instr. Meth. Phys. Res. B 351 (2015) 23.
[11] A. van Veen, H.A. Filius, J. de Vries, K.R. Bijkerk, G.J. Rozing, D. Segers, J. Nucl. Mater. 155-157 (1988) 1113.
[12] A. van Veen, J. de Vries, D. Segers, G.J. Rozing, in: P.C. Jain, R.M. Singru, K.P. Gopinathan (Eds.), Positron Annihilation, World Scientific, Singapore, 1985, p. 543.
[13] O.S. Oen, Cross Sections for Atomic Displacements in Solids by Fast Electrons, Oak Ridge National Laboratory, Oak Ridge, 1973.
[14] O.V. Ogorodnikova, V.V. Gann, M.S. Zibrov, Yu.M. Gasparyan, Phys. Procedia 71 (2015) 41.
[15] J.F. Ziegler, J.P. Biersack and U. Littmark, *The Stopping and Range of Ions in Solids* (1985) (New York: Pergamon).
[16] R.E. Stoller, M.B. Toloczko, G.S. Was, A.G. Certain, S. Dwaraknath, F.A. Garner, Nucl. Instr. Meth. Phys. Res. B 310 (2014) 75.
[17] H. Rajainmaki, Appl. Phys. A 42 (1987) 205.
[18] R. Krause-Rehberg, H.S. Leipner, Positron Annihilation in Semiconductors, Springer, 1998.
[19] S. Valkealahti, R.M. Nieminen, Appl. Phys. A 35 (1984) 51.
[20] J.V. Olsen, P. Kirkegaard, N.J. Pedersen, J. Eldrup, Phys. Stat. Sol. C 4 (2007) 4004.
[21] M.J. Puska, M. Sob, G. Brauer, T. Korhonen, J. Phys. IV France 5 (1995) C1–135.
[22] T. Troev, E. Popov, P. Staikov, T. Yoshiie, Nucl. Inst. Meth. Phys. Res. B 267 (2009) 535.
[23] W. Brandt, Positron Annihilation, Ed. By A.T. Stewart, L.O. Roeling, Academic Press, New York, 1967, p. 115.
[24] B. Bergersen, M.J. Stott, Sol. Stat. Commun. 7 (1969) 1203.
[25] D.C. Connors, R.N. West, Phys. Lett. A 30 (1969) 24.
[26] O.V. Ogorodnikova, J. Roth, M. Mayer, J. Nucl. Mater. 469 (2003) 313–316.
[27] O.V. Ogorodnikova, J. Roth, M. Mayer, J. Appl. Phys. 103 (2008) 034902.
[28] O.V. Ogorodnikova, J. Roth, M. Mayer, J. Nucl. Mater. 373 (2008) 254.
[29] Y. Kamimura, T. Tsutsumi, E. Kuramoto, Phys. Rev. B 52 (1995) 879.
[30] H.J. Wollenberger, Point defects, in: R.W. Cahn, P. Haasen (Eds.), Physical Metallurgy, North-Holland, Amsterdam, 1996, pp. 1621–1721.
[31] K. Sato, D. Itoh, T. Yoshiie, Q. Xu, A. Taniguchi, T. Toyama, J. Nucl. Mater. 417 (2011) 963.
[32] R. Frauenfelder, J. Vac. Sci. Technol. 6 (1969) 388.
[33] O.V. Ogorodnikova, M.A. Futterer, E. Serra, G. Benamati, J.-F. Salavy, G. Aiello, J. Nucl. Mater. 273 (1999) 66.
[34] O.V. Ogorodnikova, Yu. Gasparyan, V. Efimov, L. Ciupinski, J. Grzonka, J. Nucl. Mater. 451 (2014) 379.
[35] R.A. Causey, T.J. Venhaus, Phys. Script. T94 (2001) 9.
[36] O.V. Ogorodnikova, T. Tyburska, V.Kh. Alimov, K. Ertl, J. Nucl. Mater. 415 (2011) S661.
[37] J.L. Barton, Y.Q. Wang, T. Dittmar, R.P. Doerner, G.R. Tynan, Nucl. Inst. Meth. Phys. Res. B 332 (2014) 275.
[38] J. Maisonneuve, T. Oda, S. Tanaka, Fusion Sci. Technol. 60 (2011) 1507.